Chemical Science

ROYAL SOCIETY OF CHEMISTRY

EDGE ARTICLE

View Article Online
View Journal | View Issue

Cite this: *Chem. Sci.*, 2023, **14**, 5396

All publication charges for this article have been paid for by the Royal Society of Chemistry

Received 8th March 2023
Accepted 30th March 2023

DOI: 10.1039/d3sc01260c

rsc.li/chemical-science

Accurate binding of porous aluminum molecular ring catalysts with the substrate†

Dan Luo, ‡[a] Han Xiao, ‡[ab] Min-Yi Zhang, [a] Shang-Da Li, [a] Liang He, [a] Hong Lv,[a] Chun-Sen Li, [ac] Qi-Pu Lin, [a] Wei-Hui Fang *[a] and Jian Zhang [a]

Metal molecular rings are a class of compounds with aesthetically pleasing symmetry and fundamentally useful properties. The reported work generally focuses on the ring center cavity, and there is little known about those on the ring waist. Herein, we report the discovery of porous aluminum molecular rings and their performance and contribution to the cyanosilylation reaction. We develop a facile ligand induced aggregation and solvent regulation strategy towards **AlOC-58NC** and **AlOC-59NT** with high purity, high yield (75% and 70%, respectively) and gram-level scale-up. These molecular rings exhibit a "two-tier" pore feature involving the general central cavity and newly observed equatorial semi-open cavities. **AlOC-59NT** with two types of one-dimensional channels showed good catalytic activity. The interaction of the aluminum molecular ring catalyst with the substrate has been crystallographically characterized and theoretically confirmed, showing a ring adaptability process that involves the capture and binding of the substrate. This work provides new ideas for the assembly of porous metal molecular rings and to understand the overall reaction pathway involving aldehydes and is expected to inspire the design of low-cost catalysts through structural modifications.

Introduction

The creation of ring-shaped compounds has raised constant interest owing to their pleasing symmetry and fundamentally useful properties. According to the composition classification, ring-shaped compounds are organic, inorganic, and organic–inorganic hybrid ones. Organic macrocycles include crown ethers, cyclodextrins (CDs), calix[*n*]arenes, cucurbit[*n*]urils (CB[*n*]s), and pillar[*n*]arenes.[1] Toroidal inorganic clusters are normally found as polyoxometalates (POMs) like large Mo-blue wheel Mo_{154} and Mo_{176}, as well as recently reported M_{70} (M = Zr/Ce/U).[2] Hybrid rings are known as hybrid rotaxanes and a variety of metal molecular rings resulted from the abundant and flexible combination of inorganic metal nodes and organic bridges.[3] This class of rings has long fascinated chemists for its combined features and structural tunability.

From the perspective of ring type, metal molecular rings involve single-stranded rings, multiple-stranded rings or rings linked by cluster units.[4] Octametallic and hexadecametallic ferric wheels are typical single-stranded rings,[4b] while giant torus-shaped Mn_{84} (ref. 5)/Pd_{84} (ref. 4d) and Gd_{140} (ref. 6) are those constructed from clusters. Christou's group has made many efforts to synthesize single-stranded rings, including transition metal[7] and main group metal rings.[8] These rings are regarded as an ideal structural mode for understanding magnetism in elegant exchange-coupled systems. In addition to homo-metallic molecular rings, Winpenny, Christou, Powell, Zheng *et al.* contributed a lot to the research of heterometallic rings.[9] For example, alternating rare earth and transition metal heterometallic molecular rings were investigated for magnetic properties by Powell *et al.*[9d] According to the metal category, metal molecular rings currently studied include transition metals, rare earth and several main group metal rings.[4c,10] These metal ions or clusters are topologically pseudo-ditopic centers linked by ditopic chelating ligands to form cyclic structures. And bridging ligands are generally carboxylic acids, alcohol amines, pyrazoles, and alcohols, which can be used alone or together.[9d,11] We have recently been working on the isolation of a series of single-chain aluminum molecular rings through a "ligand-induced aggregation and solvent-regulation" synthetic strategy and have found that these molecular rings contain some unique porous properties with applications in host-guest chemistry and optics.[12]

Pores are the heart of a broad range of applications spanning from inorganic zeolites, macrocycles, to hybrid metal–organic

[a]*State Key Laboratory of Structural Chemistry, Fujian Institute of Research on the Structure of Matter, Chinese Academy of Sciences, 350002 Fuzhou, P. R. China*
[b]*University of Chinese Academy of Sciences, Beijing 100049, China*
[c]*Fujian Provincial Key Laboratory of Theoretical and Computational Chemistry, Xiamen, Fujian 361005, China*

† Electronic supplementary information (ESI) available: Experimental section, detailed structure charts, stability analysis, catalytic data, characterization, tables and supplement videos. CCDC 2214966 (**AlOC-58NC**), 2214967 (**AlOC-59NT**), 2214968 (**AlOC-58NC-1**) and 2214969 (**4Bz@AlOC-59NT**). For ESI and crystallographic data in CIF or other electronic format see DOI: https://doi.org/10.1039/d3sc01260c

‡ These authors contributed equally to this work.

frameworks, including gas storage, separation, and catalysis.[13] The same is true for molecular ring systems, where the central cavities are commendations for guests. And the tubular pores created by the intermolecular array packing are particularly intriguing because they afford size selectivity and unidimensional diffusion features. Therefore, although a large number of cyclic molecules have been reported, the most attention is paid to the central cavity.[14] However, the semi-open cavities through arm-like organic ligands are supposed to access guest molecules. Curiously, although the study of porous molecular clusters or porous coordination cages is still emerging in the field of cluster science,[13b] little is known about porous molecular rings containing peripheral semi-open cavities. Compared to directly using large cavity-containing ligands such as calix[*n*]arenes to construct molecular rings,[15] the use of small organic ligands has better flexibility to accommodate guests.

Encouraged by our recent discovery of the effects of solvent and ligand type on ring size and template on ring supramolecular assembly in Al(III) chemistry,[12a,b,16] we are very interested in the assembly of aluminum molecular rings. Bearing these in mind, we herein demonstrate the assembly of porous metal molecular rings and the influence of solvents on their supramolecular assembly. In addition, we discover that these porous metal molecular rings are adaptive to catalytic substrates, contributing to the catalysis efficiency and understanding the mechanism at the molecular level. The reason why we choose 3-aminoisonicotinic acid (NH_2-HIN) lies in the presence of pyridine nitrogen and the amino group could act as either a donor or acceptor for hydrogen bonding with the cluster itself and molecular guests. By using coordinating polar solvents and inert toluene, we isolated compounds $[Al_8(OH)_4(OBu^n)_8(NH_2\text{-}IN)_{12}]$ (aluminum molecular rings assembled into a nanocage structure designated as **AlOC-58NC**) and $[Al_8(OH)_8(NH_2\text{-}IN)_{16}]$ (aluminum molecular rings assembled into a nanotube structure designated as **AlOC-59NT**), respectively. They both exhibit a "two-tier" pore feature involving the central cavity and equatorial semi-open cavities. These porous rings further assemble through supramolecular interaction to form cubic and tetragonal solid-state structures. Although cubic **AlOC-58NC** has greater porosity, **AlOC-59NT** nanotube arrays with one-dimensional channels have better adsorption of substrate molecules. Combining single crystal X-ray diffraction (SCXRD) and theoretical calculations, we further illustrate the catalytic mechanism.

Results and discussion

Synthesis

The $-NH_2$ groups introduced not only increase the solubility but also have good adsorption capacity for the substrate molecules in subsequent studies. In solvothermal reactions, the choice of solvent plays a crucial role in the assembly of the porous aluminum molecular ring structures (Fig. 1). The solvothermal reaction of aluminum isopropoxide and NH_2-HIN in a stoichiometric ratio of 2 : 3 in the presence of DMF and *n*-BuOH yielded high-purity pale yellow cubic crystals $[Al_8(OH)_4(OBu^n)_8(NH_2\text{-}IN)_{12}]\cdot$(**AlOC-58NC**) (eqn (1) and Fig. S1,† about 240 mg for one batch rection). When the *n*-BuOH was removed from the system and replaced with inert toluene, pale yellow strip-like crystals $[Al_8(OH)_8(NH_2\text{-}IN)_{16}]$ (**AlOC-59NT**) were obtained (eqn (2) and Fig. S1,† about 220 mg for a one-batch reaction). These compounds can be isolated by achieving scale-up synthesis at the gram level, which provided the foundation for later performance studies (Fig. 1).

$$8Al(O^iPr)_3 + 8(n\text{-BuOH}) + 12(NH_2\text{-HIN}) + 4H_2O \rightarrow Al_8(\mu_2\text{-OH})_4(OBu^n)_8(NH_2\text{-IN})_{12}\ (\textbf{AlOC-58NC}) + 24H^iOPr \quad (1)$$

$$8Al(O^iPr)_3 + 16(NH_2\text{-HIN}) + 8H_2O \rightarrow Al_8(\mu_2\text{-OH})_8(NH_2\text{-IN})_{16}\ (\textbf{AlOC-59NT}) + 24H^iOPr \quad (2)$$

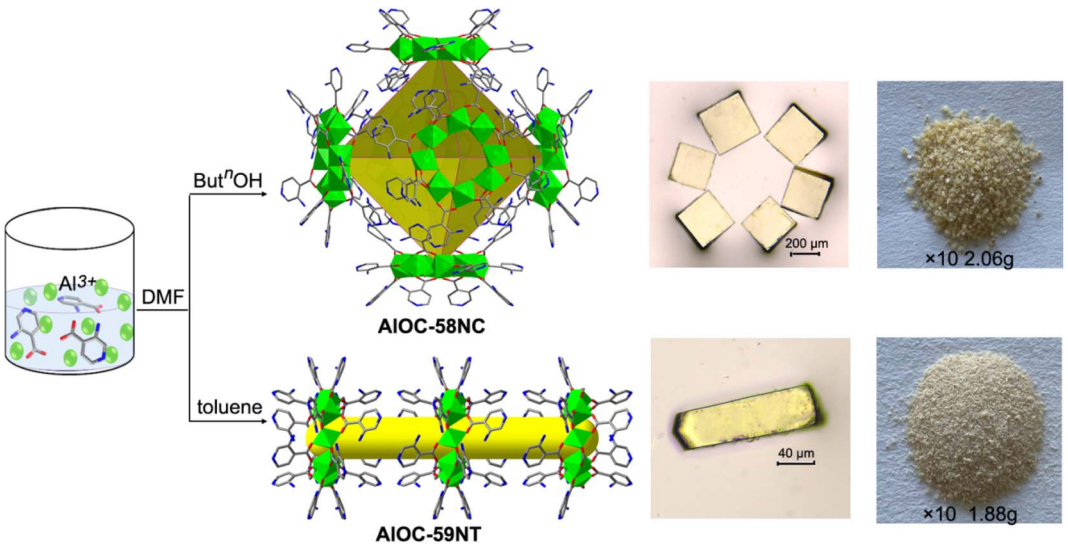

Fig. 1 Solvent-regulated synthesis strategies towards the supramolecular assembly of porous aluminum molecular rings (insets are their respective crystal photo under a microscope and scale-up synthesis).

A summary of aluminum molecular rings

In order to have a better and more comprehensive understanding of aluminum molecular rings, we summarize and analyze the rings combined with previously reported ones (Fig. 2).[12] Considering the composition (Al : $R_1(R_2)$ ratio) (R_1 = carboxylic acid; R_2 = pyrazole) and structural characteristics of rings, we divided them into four categories, including type I: $Al(MA)_2(R_1)$ (MA = monohydric alcohol) (Fig. 2a); type II: $Al(OH)_{0.5}(MA)(R_1)_{1.5}$ (Fig. 2b); type III: $Al(OH)(R_1)(R_2)$ (Fig. 2c) and type IV: $Al(OH)(R_1)_2$ (Fig. 2d). Although types III and IV possess the same Al : OH ratio, type IV is bridged by only one kind of R_1 ligand (Fig. 2d) compared to type III with both R_1 and R_2 (Fig. 2c). All Al ions in the ring have octahedral configurations and their coordination flexibility results in the formation of a diversity of molecular rings. With the increase of the Al : $R_1(R_2)$ ratio, the way how Al ions are connected has changed. The connection mode of Al ions spans from edge-sharing, *via* edge-vertex-sharing, to vertex-sharing connection. As can be seen from the side view of the ring, the introduction of the H_2N-IN ligand used herein has increased its dihedral angle with the Al ion plane and the overall height of the ring (Fig. 2e). It is worth noting that compound **AlOC-59NT** is currently the only one belonging to type IV of all rings and also has the largest dihedral angle (77°) (Fig. 2f).

Supramolecular assembly of porous aluminum molecular rings

One prominent feature of these compounds is the presence of the "two-tier" porous aluminum molecular rings. In addition to the usual ring center cavity, they have a half-open aromatic wall cavity on the waist. Each ligand hangs like an arm from a ring, and every four ligands combine to form a semi-open cavity with an aromatic wall. Since the solvent is involved in coordination with aluminum ions in **AlOC-58NC** (ring type II), there are 4 equatorial half-open cavities, while more ligands participate in the generation of the pores in **AlOC-59NT** (ring type IV), and there are as many as 8 semi-open cavities with four facing up and four facing down alternately. Their detailed supramolecular structures are discussed below.

Structure of AlOC-58NC. As shown in Fig. 3a and S3a,† there are eight *n*-BuO^- and 12 H_2N-IN ligands on the molecular ring. Eight *n*-BuO^- are suspended in the upper and lower planes of the center of the ring. Besides 8 H_2N-IN located above and below the plane of the ring (labeled as α, γ), there are additional 4 axial ligands (labeled as β). We can see two β position ligands, one α and one γ position ligands forming an open quadripartite cavity (Fig. 3b). Hence, there is a total of four such cavities within each ring. These three groups of ligands play different roles in the formation of supramolecular structures (Fig. 3c and

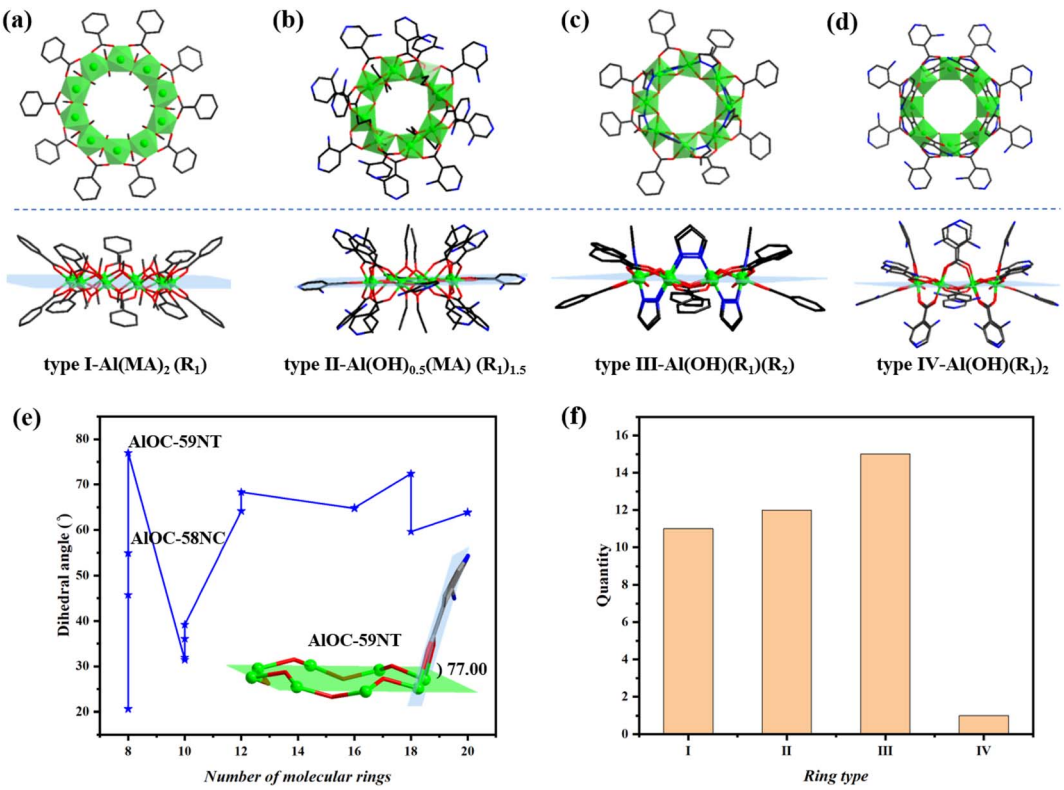

Fig. 2 Summary of current aluminum molecular rings modified by aromatic ligands. Ball-and-stick models of the top and side views for type-I (a), type-II (b), type-III (c), and type-IV (d). R_1, R_2, and MA represent carboxylic acid, pyrazole, and monohydric alcohol, respectively. H atoms have been omitted for clarity. Color code: Al, green; C, black; O, red; N, blue. (e) Summary of dihedral angles between the ring Al_n (n = 8, 10, 12, 16, 18, 20) plane and aromatic ligands calculated in macrocycles. (f) Quantitative statistics of different types of aluminum molecular rings published so far.

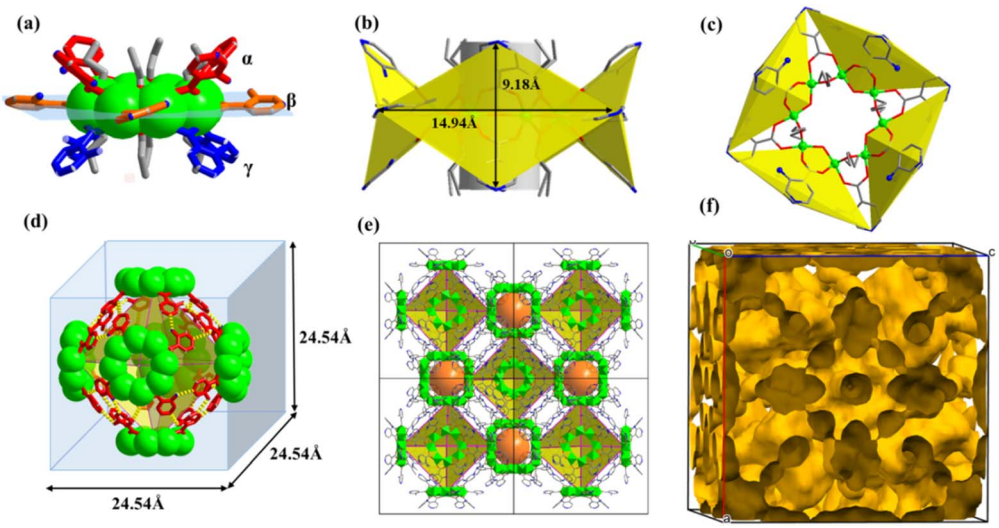

Fig. 3 Supramolecular structure of **AlOC-58NC**. (a) The side view of the ring structure (the H_2N-IN located above, on and below the plane of the Al_8 ring is labeled as α, β and γ, respectively). (b) The open quadripartite cavity consists of two β, one α and one γ position ligands (dimension: 9.18 Å × 14.94 Å). (c) The top view of the ring structure. (d) Octahedral nanocage linked by N–H···N hydrogen bonds (3.00 Å) (size: 24.54 × 24.54 × 24.54 $Å^3$). Some carbon and hydrogen atoms have been omitted for clarity. (e) Nanocage stacking diagram arranged by -ABAB- alternation. Color code: Al, green; C, black; O, red; N, blue. (f) Perspective view of the void spaces along the *b* axis.

S3a†). The α position H_2N-IN linked each other to form a mesoporous nanocage with 24 *n*-BuO^- facing inside the cage (Fig. 3d and S3b†). The β position H_2N-IN is adhesive to two nanocages, while the γ position H_2N-IN is connected to two rings on adjacent nanocages (Fig. S3c and e†). Molecular rings are usually nanotube supramolecular arrays,[4d,17] and such cage-like stacking is rare. The mesoporous nanocage structure of compound **AlOC-58NC** reminds us of previously reported **AlOC-26-NC**.[16b] **AlOC-58NC** (space group no. 211: *I*432; nanocage size 24.54 × 24.54 × 24.54 $Å^3$) possesses a higher symmetry and slightly larger size than those of **AlOC-26-NC** (ring type III, space group no. 207: *P*432; nanocage size 21.20 × 21.20 × 21.20 $Å^3$) (Fig. S4–S7†). Compared with the packing mode of the -A- alternation in **AlOC-26-NC**, the stacking of the nanocages in **AlOC-58NC** is -ABAB- alternation (6.65 Å) (Fig. 3e). Due to the presence of –N, $–NH_2$ hydrogen donors and acceptors, abundant hydrogen bond interactions (N–H···N, 3.00 Å) are included in the mesoporous nanocages (Fig. S8 and Table S1†). The nanocages compound possesses a considerable porosity of 40.5% calculated by PLATON.[18] The pore environment is provided in Fig. 3f and readers are referred to ESI Video S1† for detailed information (Fig. S9†).

Structure of AlOC-59NT. Compound **AlOC-59NT** possesses a tetragonal (space group no. 97: *I*422) nanotube array supramolecular structure (Fig. 4 and S10†). Without competition from coordinating polar solvents, there are as many as 16 H_2N-IN ligands in **AlOC-59NT**. Eight are located above and below planes of the center of the ring (labeled as the α position) and the other eight reside at the waist of the ring (labeled as the β position) (Fig. 4a and S10b†). From the top view of the ring, we can see the distribution of the α and β position ligands and there are hydrogen bonds on the ring itself (N–H···N (2.88 Å), N–H···O (2.65 Å)) (Fig. S11†). In addition to having a hollow tubular cavity (dimension: 6.62 Å × 6.62 Å × 12.67 Å), the ring itself has 8 semi-open quadrangular-conical cavities (made up of one α and three β position ligands, dimension: 9.54 Å × 14.55 Å) (Fig. 4b and S10c, d†). A better appreciation of the porous ring is provided by the surface of the two types of pores as shown in Fig. 4a and c (ESI Video S2† for detailed information).

The molecular rings give nanotubular stacks parallel to the crystal *c* axis and their neighbors, yielding a square packing with two types of channels, cylindrical channel and peanut-shaped staggering channel (Fig. 4c and d). The cylindrical channel is made up of rings in a vertical direction *via* hydrogen bond interactions between α position ligands (N–H···N (5.08 Å), C–H···N (4.54 Å), N–H···C (3.39 Å)) (Fig. S13 and S14†). Such connection within the nanotubes has not been found in all previously reported aluminum molecular rings (Fig. S15†). A cavity is enclosed by two adjacent semi-open quadrangular-conical cavities with an interleaved size of 7.0 × 10.8 $Å^2$ (Fig. 4e, S16 and S17†). Viewing down along the [−1 1 0] direction, we can see the nanotube channels formed by α position ligands and the regular aromatic channels formed by β position ligands with peanut-shaped cavities (Fig. 4f and S18†). In addition to the π···π (4.05 Å) force between β position ligands of the molecular rings on the adjacent nanotubes, there are also strong hydrogen bonds due to the presence of $–N_{py}$ and $–NH_2$ groups (N–H···N, 2.93 Å) (Fig. S19 and S20†). Although compound **AlOC-59NT** possesses a slightly small porosity compared with **AlOC-58NC** nanocages (38.8% *vs.* 40.5%), it has the highest porosity among the current aluminum nanotube arrays. The presence of such porosity is attributed to the increased number of porous cavities surrounding the ring and the larger dihedral angle (42° *vs.* 77°, defined by the ligands with the ring plane).

Compounds **AlOC-58NC** and **AlOC-59NT** remain stable in air for up to a year, which may be related to the protection of

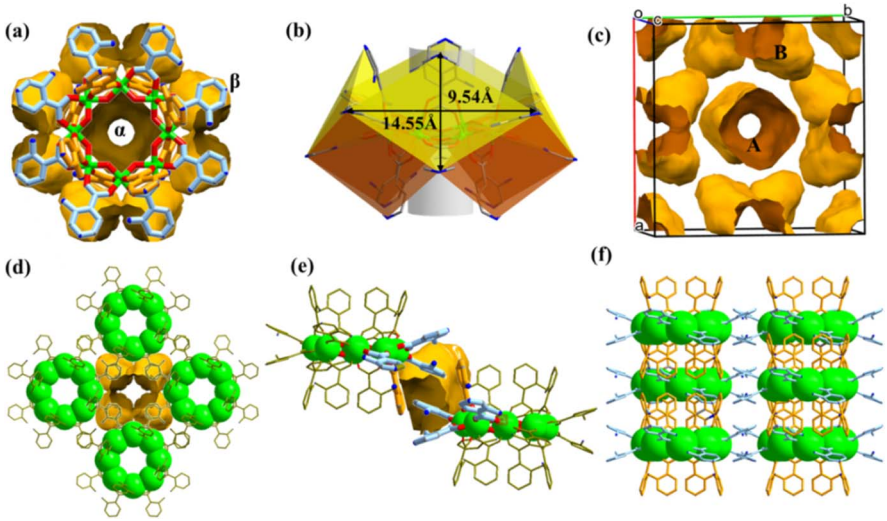

Fig. 4 Supramolecular structure of **AlOC-59NT**. (a) The surface and wire views of the ring structure (the central and surrounding H_2N-IN ligands are labeled as α and β, respectively). (b) The semi-open quadrangular-conical cavity comprises one central α and three equatorial β position ligands (dimension: 9.54 Å × 14.55 Å), the hollow tubular cavity is grey (dimension: 6.62 × 6.62 × 12.67 $Å^3$). (c) Perspective view of the two types of void spaces (A) and (B) along the *c* axis. (d) Stacking diagram of peanut-shaped cavities. (e) The peanut-shaped cavity consisting of two adjacent semi-open quadrangular-conical cavities (interleaved size: 7.0 × 10.9 $Å^2$). (f) The stacking diagram of **AlOC-59NT** along the [−1 1 0] direction showing one-dimensional aromatic walls and ladders. Color codes: Al, green; C, gray; N, blue; O, red.

aromatic ligands and the strong Al–O bond in the structure. We also refined the experimental powder X-ray diffraction (PXRD) of the compounds using the Pawley algorithm and obtained good agreement factors (R_p = 3.96%, R_{wp} = 5.91% for **AlOC-58NC**, R_p = 4.78%, R_{wp} = 7.13% for **AlOC-59NT**) (Fig. S21 and S22†). They remain stable after soaking in a low polar organic solvent for 24 h and can be dissolved in a strong polar solvent (methanol, ethanol and DMF) (Fig. S24 and S25†). However, it is unstable in an aqueous solution, which may be related to the strong hydrophilicity of amino functional groups. As shown in Fig. S26–S29,† **AlOC-59NT** has slightly better thermal stability than **AlOC-58NC**, which may be due to its stronger hydrogen bond interaction (Tables S1 and S2†). The solid-state absorption spectra indicate that they have a similar band gap, which is in line with their pale yellow color (Fig. S30 and S31†). Energy dispersive spectroscopy (EDS), Fourier transform infrared (FT-IR), bond valence sum (BVS) and element analysis qualitatively and quantitatively reveal their composition, which is consistent with the single-crystal X-ray diffraction (SCXRD) results (Fig. S32–S35, and Tables S3 and S4†).

Catalytic activity

Although a variety of molecular rings have been reported, their performances mainly focus on luminescence and magnetism, and there is also some research on photo(electro)catalysis but not organic catalysis.[19] Due to the inherent availability, sustainability, low cost and low toxicity, the development of efficient catalysts based on the main-group elements is highly desirable.[20] These porous molecular rings contain abundant hydrogen bond donors and acceptors. For example, **AlOC-59NT** contains 8 hydroxyl groups (–OH), 16 pyridine nitrogen atoms (–Npy) and 16 amino groups ($–NH_2$) (Fig. S36†). Therefore, they should contribute to guest molecule capture and thus performance improvement.[21] We chose a typical probe Lewis acid/base catalyzed cyanosilylation reaction because it involves substrate contact and adsorption.

Under the reaction conditions of 1.5 mol% catalyst loading, 30 °C and 2 h of reaction time, **AlOC-58NC** and **AlOC-59NT** showed obvious catalytic activity (Fig. 5). With 20 mg of AlOC crystals used as the catalyst, **AlOC-58NC** and **AlOC-59NT** afford yields of 80% and 92%, respectively (Table S6,† entries 1–2). Control experiments indicated the effectiveness of the catalysts and aluminum ions were likely to be the active sites and 3-aminoisonicotinic acid may have a positive synergistic effect (Table S6,† entries 3–5). Kinetic curves further showed that **AlOC-59NT** not only has a higher yield but also a faster reaction rate compared to **AlOC-58NC** (Fig. S37†). To test their performances in catalyzing cyanosilylation reactions, several substituted benzaldehydes were introduced as the substrates (Fig. 5b). It is worth noting that the electron-withdrawing functional group (such as 4-trifluoromethylbenzaldehyde and 3-fluorobenzaldehyde) is helpful (Table S6,† entries 6–9), while the electron donating group (4-methoxybenzaldehyde) reduced the yield of the reaction for the same time (Table S6,† entries 10–11). Sequential reactions show that the activity of the recovered catalysts did not decrease significantly after 3 cycles (Fig. S38–S40†).

To further understand the in-depth mechanism, we performed the soaking experiment of the catalyst with a representative substrate benzaldehyde solution. Both compounds still retain the crystal quality to carry out further SCXRD, which shows that **AlOC-59NT** has better adsorption capacity than **AlOC-58NC** under the same conditions. Their structures (designated as **AlOC-58NC-1** and **4Bz@AlOC-59NT**) can be solved and refined in the same space group but with slight changes in crystal parameters (Tables S7 and

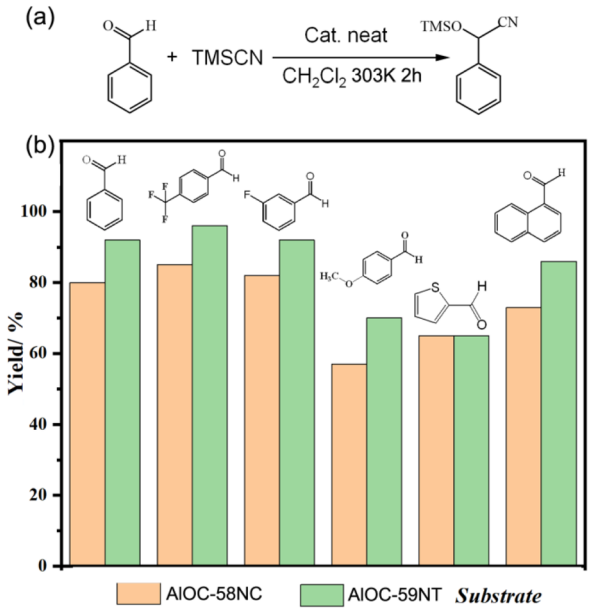

Fig. 5 Results of the cyanosilylation of aldehyde in the presence of AlOCs. (a) Reaction conditions: catalyst **AlOC-58NC**, **AlOC-59NT** 1.5% mol, aldehyde 0.5 mmol, TMSCN 1 mmol, solvent CH_2Cl_2, temperature (303 K) under N_2. Yields were determined by ^1H NMR using CH_2Br_2 as an internal standard. (b) Substrate scope for reaction and catalytic performance comparison between **AlOC-58NC** and **AlOC-59NT**.

S8†). No suitable Q peak was found in **AlOC-58NC**, but obvious electron cloud density near the aromatic ring was found in **AlOC-59NT**, which was assigned to halves of benzaldehyde (designated as **4Bz@AlOC-59NT**) (Fig. 6a and S40a†). Each molecular ring traps 8 benzaldehyde molecules *via* π···π (3.85 Å) and N–H···C (3.63–4.32 Å) hydrogen bonding interactions (Fig. S41b†). Two adjacent molecular rings share a benzaldehyde guest through π···π (3.85 Å) interaction (Fig. S42a†). The adjacent benzaldehyde guest is stabilized by C–H···O (4.29 Å) hydrogen bond interaction (Fig. S43b†) (ESI Video S3† for detailed information). Interactions between the host and captured guests were also calculated by Hirshfeld surface d_{norm} mapping, indicating a strong interaction in compound **4Bz@AlOC-59NT** (Fig. S45 and S46†). Besides, several differences were observed in **4Bz@AlOC-59NT** when compared with the pristine crystal. After the catalytic substrate enters the semi-open quadrangular-conical cavity, the twist angle of aromatic ligands on it changes to varying degrees (Fig. S47†). The dimensions of the cavity change accordingly (dimension: 9.54 × 14.55 Å^2 *vs.* 9.95 × 14.49 Å^2) (Fig. S48†). The peanut-shaped cavity is also enlarged (7.0 × 10.8 Å^2 *vs.* 7.2 × 11.02 Å^2) (Fig. S49†). The presence of benzaldehyde in **4Bz@AlOC-59NT** was further confirmed by ^1H NMR, FT-IR and PXRD (Fig. S50–S52†).

Theoretical calculations were employed for the deep mining of capture information (Fig. 6c). Our calculation results are well in consistence with the soaking experiment where **AlOC-59NT** is demonstrated to have better adsorption capacity than **AlOC-58NC**. In their most stable adsorption conformation, the calculated adsorption energy of **AlOC-59NT** is −15.8 kcal mol^{-1}, which is much lower than that of **AlOC-58NC** (−9.6 kcal mol^{-1}) (Fig. S52 and S53†). In addition, the location of benzaldehyde in the calculated results is exactly the one in the soaking experimental results, where the benzaldehyde is adhesive to **AlOC-59NT** through four aromatic rings with strong hydrogen bonding and π···π

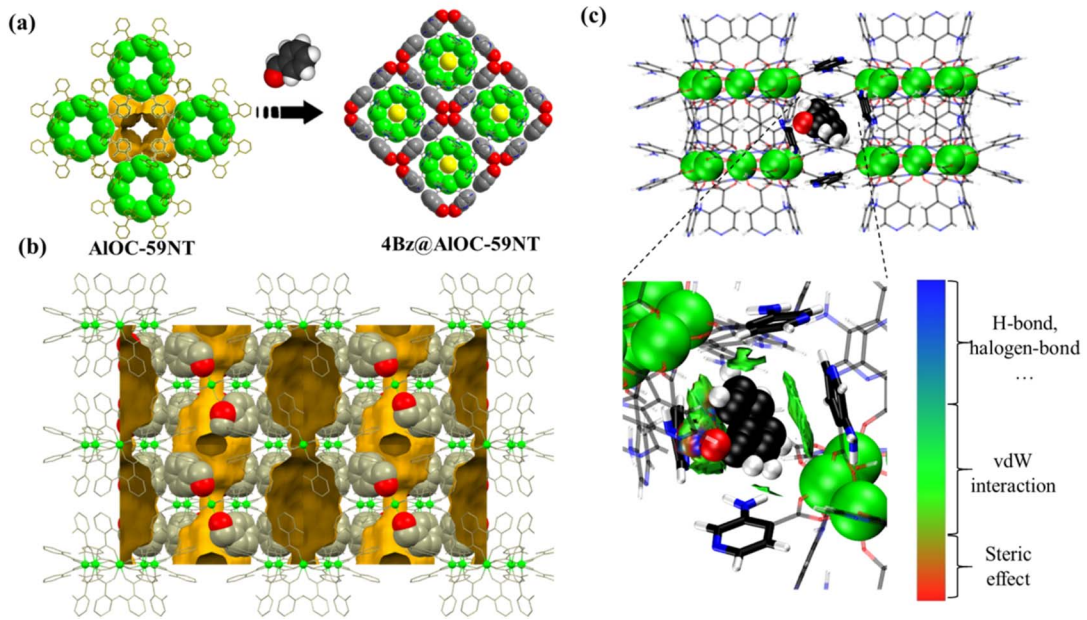

Fig. 6 Crystallography visualization and theoretical calculation results of the immersion experiment of the catalyst and substrate. (a) Schematic diagram of the immersion experiment; (b) detailed location of the benzaldehyde substrate; (c) theoretical calculation showing the adsorption site derived from the theoretical calculation in **AlOC-59NT**, as well as weak interactions between the catalyst and substrate. Atom color codes: Al, green; Fe, cyan; C, gray; N, blue; O, red.

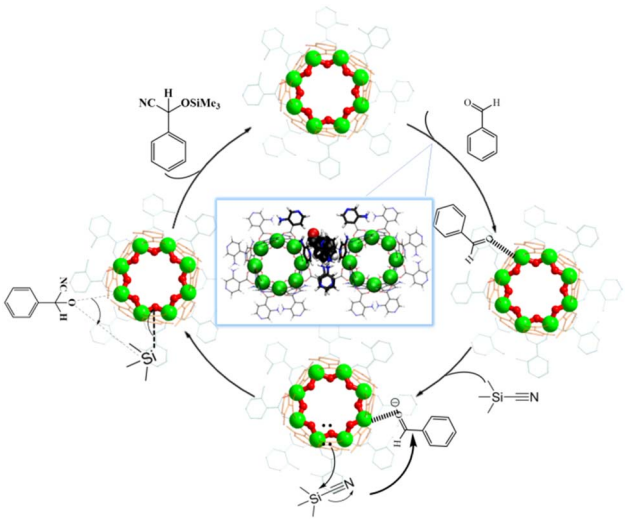

Scheme 1 Proposed mechanism for the cyanosilylation reaction of aldehyde compounds catalyzed by porous aluminum molecular rings.

interactions. The adaptivity of the rings to benzaldehyde is also proved by theoretical calculation (see ESI Video S4†). Moreover, the molecular ring of **AlOC-59NT** is calculated to have slightly stronger Lewis acid/base characteristics than those of **AlOC-58NC** (Fig. S55†). It is reported that the formation of the cyanosilylation products involves the activation of carbonyl compounds and silyl compounds by Lewis acid sites and Lewis bases, respectively.[22] Here, Al^{3+} with strong Lewis acidity first activates the substrate aldehyde to form a weak donor–acceptor adduct, and then the hydroxyl functional group acting as a Lewis base activates TMSCN to obtain the cyanosilylation product (Scheme 1). The abundant amino functional group sites and pyridine nitrogen atoms in the structure help to confine the substrate to the catalyst cavity, which is more accessible to Al^{3+}. Moreover, the regular and ordered one-dimensional hydroxyl channels accelerate the activation of TMSCN, which synergistically improve the catalyst activity. Combining theoretical calculations with experimental results, we reveal that the catalytic effect is not only related to Lewis acid/base characteristics but also to the adsorption capacity.

Conclusions

In summary, we have developed a method for preparing porous molecular rings and used solvent-controlled methods to regulate the type of pores. **AlOC-58NC** possesses a nanocage structure with a larger porosity, while compound **AlOC-59NT** is a nanotube with two types of channels. They both present high stabilities and catalytic activity toward cyanosilylation reactions. Among them, **AlOC-59NT** with one-dimensional channels showed good catalytic activity. The interaction between the catalyst and substrate was further crystallographically characterized and theoretically confirmed, showing a structural adaptability process that involves the binding of the guests in **AlOC-59NT**. This research provides a method for constructing novel porous materials and contributes to helping understand mechanisms in the field of catalysis. In addition, this type of porous cluster should also be applied to a wide range of areas such as selective adsorption separation.

Data availability

The datasets supporting this article have been uploaded as part of the ESI. X-ray crystallographic data for the structures reported in the article have been deposited at the Cambridge Crystallographic Data Centre, under deposition numbers CCDC 2214966 (**AlOC-58NC**), 2214967 (**AlOC-59NT**), 2214968 (**AlOC-58NC-1**), and 2214969 (**4Bz@AlOC-59NT**). Copies of the data can be obtained free of charge *via* **https://www.ccdc.cam.ac.uk/structures/**. The datasets are also provided as Supplementary datasets with this paper. All other data supporting the findings of this study are available within the paper and its ESI†, and from the corresponding author.

Author contributions

All authors contributed extensively to the work presented in this paper. J. Zhang and W.-H. Fang conceived the research project. D. Luo performed the synthesis, characterization and catalytic experiments. H. Xiao performed theoretical calculations. H. Lv and S.-D. Li assisted with conceiving catalytic experiments. M.-Y. Zhang and C.-S. Li assisted with conceiving theoretical calculations. L. He and Q.-P. Lin performed Rietveld and Pawley fit refinement on the experimental powder PXRD patterns of compounds. W.-H. Fang and D. Luo wrote the manuscript and ESI† with input from the other authors.

Conflicts of interest

There are no conflicts to declare.

Acknowledgements

Research reported in this publication was supported by the National Natural Science Foundation of China (92061104 and 21933009), National Key Research and Development Project (2022YFA1503900), Natural Science Foundation of Fujian Province (2021J06035, 2021J01525) and Youth Innovation Promotion Association CAS (Y2021081).

Notes and references

1 (*a*) D. J. Cram and J. M. Crram, *Science*, 1974, **183**, 803–809; (*b*) J.-M. Lehn, *Science*, 1993, **260**, 1762–1963; (*c*) C. J. Pedersen, *Science*, 1998, **241**, 536–540; (*d*) E. A. Appel, J. del Barrio, X. J. Loh and O. A. Scherman, *Chem. Soc. Rev.*, 2012, **41**, 6195–6214; (*e*) L. Isaacs, *Acc. Chem. Res.*, 2014, **47**, 2052–2062; (*f*) K. Jie, Y. Zhou, Y. Yao and F. Huang, *Chem. Soc. Rev.*, 2015, **44**, 3568–3587.

2 (*a*) A. Müller, E. Krickemeyer, H. Bögge, M. Schmidtmann, C. Beugholt, P. Kögerler and C. Lu, *Angew. Chem., Int. Ed.*, 1998, **37**, 1220–1223; (*b*) T. Liu, E. Diemann, H. Li, A. W. M. Dress and A. M. ller, *ChemInform*, 2004, **35**, 59–62; (*c*) H. Imai, T. Akutagawa, F. Kudo, M. Ito, K. Toyoda,

S. Noro, L. Cronin and T. Nakamura, *J. Am. Chem. Soc.*, 2009, **131**, 13578–13579; (*d*) S. Oien-Odegaard, C. Bazioti, E. A. Redekop, O. Prytz, K. P. Lillerud and U. Olsbye, *Angew. Chem., Int. Ed.*, 2020, **59**, 21397–21402; (*e*) I. Colliard and M. Nyman, *Angew. Chem., Int. Ed.*, 2021, **60**, 7308–7315.

3 (*a*) G. A. Timco, E. J. McInnes and R. E. Winpenny, *Chem. Soc. Rev.*, 2013, **42**, 1796–1806; (*b*) Y. Z. Zheng, G. J. Zhou, Z. Zheng and R. E. Winpenny, *Chem. Soc. Rev.*, 2014, **43**, 1462–1475; (*c*) E. J. L. McInnes, G. A. Timco, G. F. S. Whitehead and R. E. P. Winpenny, *Angew. Chem., Int. Ed.*, 2015, **54**, 14244–14269.

4 (*a*) M. Manoli, R. Inglis, M. J. Manos, V. Nastopoulos, W. Wernsdorfer, E. K. Brechin and A. J. Tasiopoulos, *Angew. Chem., Int. Ed.*, 2011, **50**, 4441–4444; (*b*) L. F. Jones, A. Batsanov, E. K. Brechin, D. Collison, M. Helliwell, T. Mallah, E. J. L. McInnes and S. Piligkos, *Angew. Chem., Int. Ed.*, 2002, **41**, 4318–4321; (*c*) X.-Y. Zheng, J. Xie, X.-J. Kong, L.-S. Long and L.-S. Zheng, *Coord. Chem. Rev.*, 2019, **378**, 222–236; (*d*) R. A. Scullion, A. J. Surman, F. Xu, J. S. Mathieson, D. L. Long, F. Haso, T. Liu and L. Cronin, *Angew. Chem., Int. Ed.*, 2014, **53**, 10032–10037.

5 A. J. Tasiopoulos, A. Vinslava, W. Wernsdorfer, K. A. Abboud and G. Christou, *Angew. Chem., Int. Ed.*, 2004, **43**, 2117–2121.

6 X. Y. Zheng, Y. H. Jiang, G. L. Zhuang, D. P. Liu, H. G. Liao, X. J. Kong, L. S. Long and L. S. Zheng, *J. Am. Chem. Soc.*, 2017, **139**, 18178–18181.

7 (*a*) C. Canada-Vilalta, M. Pink and G. Christou, *Chem. Commun.*, 2003, 1240–1241; (*b*) K. H. K. Lee, L. Aebersold, J. E. Peralta, K. A. Abboud and G. Christou, *Inorg. Chem.*, 2022, **61**, 17256–17267.

8 (*a*) P. King, T. C. Stamatatos, K. A. Abboud and G. Christou, *Angew. Chem., Int. Ed.*, 2006, **45**, 7379–7383; (*b*) T. C. Stamatatos, S. Mukherjee, K. A. Abboud and G. Christou, *Chem. Commun.*, 2008, **1**, 62–64.

9 (*a*) G. A. Timco, T. B. Faust, F. Tuna and R. E. Winpenny, *Chem. Soc. Rev.*, 2011, **40**, 3067–3075; (*b*) A. Fernandez, J. Ferrando-Soria, E. M. Pineda, F. Tuna, I. J. Vitorica-Yrezabal, C. Knappke, J. Ujma, C. A. Muryn, G. A. Timco, P. E. Barran, A. Ardavan and R. E. Winpenny, *Nat. Commun.*, 2016, **7**, 10240; (*c*) I. A. Kühne, C. E. Anson and A. K. Powell, *Front. Chem.*, 2020, **8**; (*d*) D. Schray, G. Abbas, Y. Lan, V. Mereacre, A. Sundt, J. Dreiser, O. Waldmann, G. E. Kostakis, C. E. Anson and A. K. Powell, *Angew. Chem., Int. Ed.*, 2010, **49**, 5185–5188.

10 (*a*) G. E. Kostakis, A. M. Ako and A. K. Powell, *Chem. Soc. Rev.*, 2010, **39**, 2238–2271; (*b*) G. E. Kostakis, S. P. Perlepes, V. A. Blatov, D. M. Proserpio and A. K. Powell, *Coord. Chem. Rev.*, 2012, **256**, 1246–1278; (*c*) X. Y. Zheng, X. J. Kong, Z. Zheng, L. S. Long and L. S. Zheng, *Acc. Chem. Res.*, 2018, **51**, 517–525.

11 (*a*) M. H. Du, S. H. Xu, G. J. Li, H. Xu, Y. Lin, W. D. Liu, L. S. Long, L. S. Zheng and X. J. Kong, *Angew. Chem., Int. Ed.*, 2022, **61**, e202116296; (*b*) H. L. Zhang, Y. Q. Zhai, H. Nojiri, C. Schroder, H. K. Hsu, Y. T. Chan, Z. Fu and Y. Z. Zheng, *J. Am. Chem. Soc.*, 2022, **144**, 15193–15202; (*c*) E. E. Moushi, C. Lampropoulos, W. Wernsdorfer, V. Nastopoulos, G. Christou and A. J. Tasiopoulos, *J. Am. Chem. Soc.*, 2010, **132**, 16146–16155; (*d*) C. P. Raptopoulou, V. Tangoulis and E. Devlin, *Angew. Chem., Int. Ed.*, 2002, **41**.

12 (*a*) L. Geng, C. H. Liu, S. T. Wang, W. H. Fang and J. Zhang, *Angew. Chem., Int. Ed.*, 2020, **59**, 16735–16740; (*b*) Y. Li, C. Zheng, S. T. Wang, Y. J. Liu, W. H. Fang and J. Zhang, *Angew. Chem., Int. Ed.*, 2022, **61**, e202116563; (*c*) S. T. Wang, Y. J. Liu, C. C. Feng, W. H. Fang and J. Zhang, *Aggregate*, 2022, DOI: **10.1002/agt2.264**; (*d*) Y. J. Liu, Y. F. Sun, S. H. Shen, S. T. Wang, Z. H. Liu, W. H. Fang, D. S. Wright and J. Zhang, *Nat. Commun.*, 2022, **13**, 6632.

13 (*a*) N. Hanikel, X. Pei, S. Chheda, H. Lyu, W. Jeong, J. Sauer, L. Gagliardi and O. M. Yaghi, *Science*, 2021, **374**, 454–459; (*b*) L. Qin, Y. Z. Yu, P. Q. Liao, W. Xue, Z. Zheng, X. M. Chen and Y. Z. Zheng, *Adv. Mater.*, 2016, **28**, 10772–10779; (*c*) F. Jin, E. Lin, T. Wang, D. Yan, Y. Yang, Y. Chen, P. Cheng and Z. Zhang, *Chem*, 2022, **8**, 3064–3080; (*d*) X. Zhao, Q. Yin, X. Mao, C. Cheng, L. Zhang, L. Wang, T. F. Liu, Y. Li and Y. Li, *Nat. Commun.*, 2022, **13**, 2721–2728; (*e*) J. Zhou, G. C. Yu, Q. Li, M. B. Wang and F. H. Huang, *J. Am. Chem. Soc.*, 2020, **142**, 2228–2232.

14 (*a*) C.-Y. Cheng, T. C. Stamatatos, G. Christou and C. R. Bowers, *J. Am. Chem. Soc.*, 2010, **132**, 5387–5393; (*b*) K. Hong and H. Chun, *Inorg. Chem.*, 2013, **52**, 9705–9707.

15 (*a*) S. Wang, X. Gao, X. Hang, X. Zhu, H. Han, X. Li, W. Liao and W. Chen, *J. Am. Chem. Soc.*, 2018, **140**, 6271–6277; (*b*) T. Kajiwara, H. Wu, T. Ito, N. Iki and S. Miyano, *Angew. Chem., Int. Ed.*, 2004, **43**, 1832–1835.

16 (*a*) L. Geng, C. H. Liu, S. T. Wang, W. H. Fang and J. Zhang, *Angew. Chem., Int. Ed.*, 2020, **59**, 16735–16740; (*b*) S. S. Yao, W. H. Fang, Y. Sun, S. T. Wang and J. Zhang, *J. Am. Chem. Soc.*, 2021, **143**, 2325–2330.

17 Z. Wang, H. F. Su, Y. W. Gong, Q. P. Qu, Y. F. Bi, C. H. Tung, D. Sun and L. S. Zheng, *Nat. Commun.*, 2020, **11**, 308.

18 S. Christensen, N. Bindzus, M. Christensen and B. Brummerstedt Iversen, *Acta Crystallogr., Sect. C: Struct. Chem.*, 2015, **71**, 9–19.

19 (*a*) W. T. Jin, F. Yang, L. Deng, M. L. Chen, J. F. Chen, H. B. Chen and Z. H. Zhou, *Inorg. Chem.*, 2018, **57**, 14116–14122; (*b*) S. Wang, X. Gao, X. Hang, X. Zhu, H. Han, X. Li, W. Liao and W. Chen, *J. Am. Chem. Soc.*, 2018, **140**, 6271–6277; (*c*) T. Ghosh, G. Christou and G. Maayan, *Angew. Chem., Int. Ed.*, 2019, **58**, 6476–6480; (*d*) W. P. Chen, P. Q. Liao, P. B. Jin, L. Zhang, B. K. Ling, S. C. Wang, Y. T. Chan, X. M. Chen and Y. Z. Zheng, *J. Am. Chem. Soc.*, 2020, **142**, 4663–4670.

20 (*a*) A. L. Liberman-Martin, R. G. Bergman and T. D. Tilley, *J. Am. Chem. Soc.*, 2015, **137**, 5328–5331; (*b*) S. Rawat, M. Bhandari, B. Prashanth and S. Singh, *ChemCatChem*, 2020, **12**, 2407–2411; (*c*) S. Yadav, R. Dixit, K. Vanka and S. S. Sen, *Chem.–Eur. J.*, 2018, **24**, 1269–1273; (*d*) Z. Yang, M. Zhong, X. Ma, S. De, C. Anusha, P. Parameswaran and H. W. Roesky, *Angew. Chem., Int. Ed.*, 2015, **54**, 10225–10229; (*e*) E. Tzadka Bukhaltsev, I. Goldberg and A. Vigalok, *Chem. Commun.*, 2009, 2041–2043; (*f*) T. Kundu, J. Wang, Y. Cheng, Y. Du, Y. Qian, G. Liu and D. Zhao, *Dalton Trans.*, 2018, **47**, 13824–13829; (*g*) Y. Li, Z. Chang,

F. Huang, P. Wu, H. Chu and J. Wang, *Dalton Trans.*, 2018, **47**, 9267–9273.

21 (*a*) Q. Huang, Y. Hu, Y. Pei, J. Zhang and M. Fu, *Appl. Catal., B*, 2019, **259**, 118106; (*b*) X. L. Jiang, Y. E. Jiao, S. L. Hou, L. C. Geng, H. Z. Wang and B. Zhao, *Angew. Chem., Int. Ed.*, 2021, **60**, 20417–20423.

22 L. M. Aguirre-Diaz, M. Iglesias, N. Snejko, E. Gutierrez-Puebla and M. A. Monge, *Chem.–Eur. J.*, 2016, **22**, 6654–6665.